ChemPubSoc Europe

DOI: 10.1002/chem.201503166

CHEMISTRY A European Journal Full Paper

Imaging Agents

Multi-Functionalized Carbon Nano-onions as Imaging Probes for Cancer Cells

Marco Frasconi,[a] Roberto Marotta,[b] Lyn Markey,[c] Kevin Flavin,[c] Valentina Spampinato,[d] Giacomo Ceccone,[d] Luis Echegoyen,[e] Eoin M. Scanlan,[c] and Silvia Giordani*[a]

Abstract: Carbon-based nanomaterials have attracted much interest during the last decade for biomedical applications. Multimodal imaging probes based on carbon nano-onions (CNOs) have emerged as a platform for bioimaging because of their cell-penetration properties and minimal systemic toxicity. Here, we describe the covalent functionalization of CNOs with fluorescein and folic acid moieties for both imaging and targeting cancer cells. The modified CNOs display high brightness and photostability in aqueous solutions and their selective and rapid uptake in two different cancer cell lines without significant cytotoxicity was demonstrated. The localization of the functionalized CNOs in late-endosomes cell compartments was revealed by a correlative approach with confocal and transmission electron microscopy. Understanding the biological response of functionalized CNOs with the capability to target cancer cells and localize the nanoparticles in the cellular environment, will pave the way for the development of a new generation of imaging probes for future biomedical studies.

Introduction

The investigation of novel nano-platforms capable of carrying therapeutic agents and with recognition capabilities for specific targeting and optical outputs for imaging is of major interest in the treatment of cancer[1,2] and of other types of infections, such as HIV.[3] Indeed, active targeting of therapeutic agents toward cancer cells plays a key role in enhancing the overall bioavailability of nanomaterials. Strategies for selective targeting employ ligands that bind specifically to receptors that are overexpressed on the cancer cell membrane relative to those of normal cells: the interaction with the cell surface is the one that defines the biodistribution of the therapeutic agent in vivo.[1,4] Indeed, the surface composition of the nanomaterials is critical in determining their interaction with the biological system. A proper balance of targeting and imaging units on the particle's surface that allows precise control of the circulation times, passive accumulation and retention at the site of action and active cellular uptake at the same time, can offer optimal therapeutic outcomes.[5] Carbon-based nanomaterials,[6] such as carbon nanotubes (CNTs),[7–12] carbon nanohorns (CNHs),[13] nanodiamonds (NDs),[14,15] fullerenes[16] and carbon nano-onions (CNOs),[17] have emerged as one of the most promising classes of scaffold nanomaterials for imaging, diagnostic and therapeutic applications.[18–20] Extensive biological studies on different carbon nanomaterials have shown significant differences in the internalization pathway and the biological activity in cancer cells for the different nanomaterial properties. The chemical functionalization of the surface of these materials can be achieved through a variety of different synthetic strategies,[21–23] which allows for optimal surface distribution of the functional groups. Different strategies have been reported for the multiple surface functionalization of CNTs[24] and NDs[25] by using diazonium salts generated in situ.

One approach to introduce surface functionalities on these nanomaterials involves the chemical modification of their surfaces. Among different carbon-based nanomaterials, multi-shell fullerenes, known as carbon nano-onions,[17,26,27] are especially promising as a platform for chemical modification with targeting units for biomedical studies, since they are small enough (average diameters of 5 nm) to be transported in the circulatory system with high biocompatibility and minimal systemic toxicity.[17] We have recently demonstrated that grafting the surface of CNOs with water-soluble moieties results in: 1) low inflammation in vitro, with a significant reduction in the secretion of cytokines IL-1β, and 2) decrease in the recruitment of

[a] Dr. M. Frasconi, Prof. Dr. S. Giordani
Istituto Italiano di Tecnologia (IIT), Nano Carbon Materials Laboratory
Via Morego 30, 16163 Genova (Italy)
E-mail: silvia.giordani@iit.it

[b] Dr. R. Marotta
Istituto Italiano di Tecnologia (IIT), Electron Microscopy Laboratory
Via Morego 30, 16163 Genova (Italy)

[c] Dr. L. Markey, Dr. K. Flavin, Dr. E. M. Scanlan
Trinity College Dublin, The University of Dublin
Trinity Biomedical Science Institute, School of Chemistry
152-160 Pearse Street, Dublin 2 (Ireland)

[d] Dr. V. Spampinato, Dr. G. Ceccone
European Commission, Joint Research Centre
Institute for Health and Consumer Protection
Via E. Fermi 2749, 21027 Ispra, Varese (Italy)

[e] Prof. Dr. L. Echegoyen
University of Texas at El Paso (UTEP), Department of Chemistry
El Paso, Texas 79968 (USA)

Supporting information and ORCID(s) from the author(s) for this article are available on the WWW under http://dx.doi.org/10.1002/chem.201503166.

neutrophils and monocytes after injection in mice.[16] A lower inflammatory potential was also observed for CNOs compared to CNTs modified with similar functional groups.[16] The results obtained in these toxicological studies have encouraged the investigation of fluorescent labelled CNOs as probes for the high resolution imaging of intracellular trafficking and studies of biodistribution in different cell lines, including MCF-7 human breast cancer cells[26] and HeLa Kyoto cells.[29]

The surface modification of CNOs still remains a critical determinant for their interactions at the biointerfaces and for active intracellular delivery. With the aim of developing an efficient imaging probe that can be used to direct the binding of functionalized CNOs to receptors that are highly overexpressed by cancer cells relative to normal cells and to maximize their selectivity, we have designed multifunctional CNOs bearing folic acid as a targeting moiety, and fluorescein as an imaging agent. Folic acid was chosen as the targeting agent due to its high binding affinity to the folate receptors ($K_d \sim 0.1$ nM), which are frequently overexpressed in a range of tumour cells. Because of its properties, folic acid has gained substantial interest as a ligand for cancer targeting.[30–32] Folic acid has been used as a targeting agent combined with different materials including liposomes, protein toxins, metals and polymeric nanoparticles, linear polymers, and dendrimers to deliver drugs selectively into cancer cells using folate-receptor-mediated endocytosis.[33–35] Due to its high fluorescence quantum yield and low toxicity fluorescein has been widely used as dye for the functionalization of nanomaterials.[8a,17,19] In the present study, we have focused our attention on CNOs as highly robust and tuneable platforms for targeting cancer cells. In our design of multifunctional imaging systems, CNOs with a diameter of 5 nm are particularly attractive because, in addition to enabling penetration into solid tumours, they can be readily chemically modified. The outer shell of CNOs possesses reactive sites that are suitable for functionalization and offers a reasonable surface area for the attachment of a wide range of imaging, targeting and/or therapeutic agents. Herein, we demonstrate the functionalization of these carbon-based nanoparticles with two different moieties by treatment of pristine CNOs with two in situ prepared aryl diazonium salts, that allow the grafting of benzoic acid and alkyne functionalities on the surface of the CNOs (Scheme 1).

Folic acid was introduced by the condensation reaction of a primary amine with the benzoic acid unit on the CNOs while the attachment of fluorescein was accomplished by a copper catalysed azide–alkyne Huisgen cycloaddition (CuAAC) onto an alkyne functionality (Scheme 2).

The surface morphology and chemical composition of the CNOs were characterized by high-resolution transmission electron microscopy (HRTEM), thermal gravimetric analysis (TGA), attenuated total reflectance Fourier transform infrared (ATR-FTIR) and Raman spectroscopies. We have also employed time-of-flight secondary ion mass spectrometry (ToF-SIMS) and X-ray photoelectron spectroscopy (XPS) to characterize the surface chemistry of the modified CNOs in the different phases of the functionalization. XPS and ToF-SIMS have been widely used for the characterization of the chemical composition of functionalized surfaces[36–38] and nanomaterials,[39,40] providing fundamental information for their successful implementation in biomedical applications.

The CNO constructs were tested towards HeLa and KB cells, a human nasopharyngeal epidermal carcinoma that expresses the folate receptor, and their cytotoxicity was assessed. The specificity of the CNOs modified with folic acid was evaluated by confocal microscopy, revealing an enhanced uptake by cancer cells having overexpressed folate receptors compared to CNOs without the targeting agent.[41] The integration of the results from confocal microscopy with transmission electron microscopy (TEM) imaging allowed us to develop a correlative light and electron microscopy (CLEM) approach to investigate the behaviour of carbon-based nanomaterials in cells. The CLEM analysis combines the advantages of typically independent but powerful microscopic techniques and can be recognize as method of choice when targeting specific events in large populations of cells or tissues.[34] Using electron microscopy we corroborated the results from confocal analysis that showed the internalization of the folate-conjugated CNOs via an endocytosis pathway. The selective and rapid internalization of the

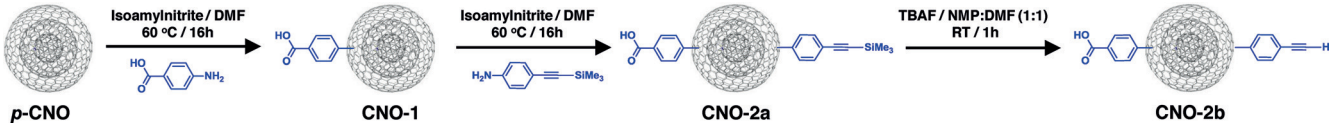

Scheme 1. Procedure for the synthesis of dual-functionalized CNOs.

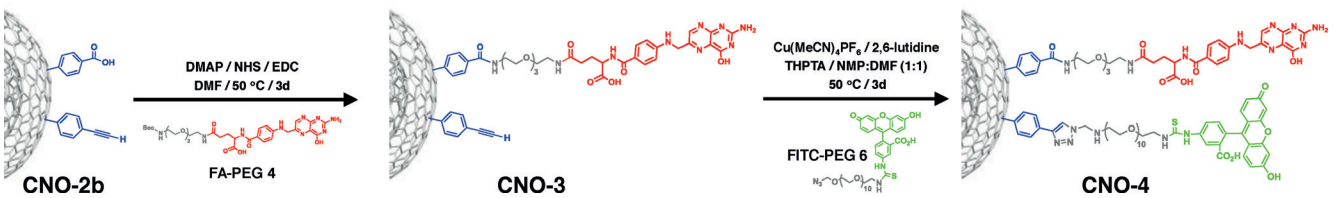

Scheme 2. Synthetic procedure for the covalent functionalization of **CNO-2b** with the folic acid unit (**FA-PEG 4**) by amide coupling and with the fluorescein unit (**FITC-PEG 6**) by copper catalysed azide–alkyne Huisgen cycloaddition (CuAAC) to yield **CNO-4**.

CNOs by cancer cells overexpressing the folate receptor results from the functionalization of the CNOs with the targeting unit as well as from the small dimensions of the particle itself. These results clearly indicate that the modified CNOs provide valuable platforms to develop imaging probes for cancer cells in biomedical studies.

Results and Discussion

The synthesis of the multifunctional CNOs starts (Scheme 1) with the pristine CNOs (**p-CNO**) which are subjected to a series of reactions with diazonium salts[21] to covalently functionalize the **p-CNO** with: 1) benzoic acid groups, which act as reactive sites for the amide-coupling reaction with the modified folic acid unit (**FA-PEG 4**), and 2) phenylacetylene moieties, which can then undergo CuAAC ligation to attach the fluorescein unit (**FITC-PEG 6**) on the surface of the CNO. The targeting ligand and the fluorescent unit were both conjugated with a polyethylene glycol chain in order to enhance their solubility and to introduce a spacer between the functional units and the CNOs surface (see the Supporting Information for detailed synthetic procedures and characterization). The surface of the CNOs was first decorated with carboxylic acid groups to obtain **CNO-1**, by reacting the **p-CNO** with 4-amino benzoic acid in the presence of isoamyl nitrite, following a previously reported procedure.[11] The benzoic acid functionalized **CNO-1** were collected from the reaction mixture by centrifugation and washed with water, before being treated with 4-((trimethylsilyl)ethynyl)aniline in a second diazonium reaction to produce **CNO-2 a**. The deprotection of the silyl group from the phenylacetylene was performed by treating the **CNO-2 a** in a solution containing *tert*-butyldimethylsilyl ethers (TBA) at room temperature to yield the **CNO-2 b**, which contains benzoic acid and phenylacetylene groups.

The surface chemical composition at the different phases of the CNOs functionalization was probed by XPS analysis (see the Supporting Information for experimental details). The elemental information on the surface of the CNO samples was obtained from the survey spectra (Figure S2 in the Supporting Information) and the compositions of the different elements are reported in Table 1. The investigation of the **p-CNO** reveals the presence of a small amount of oxygen and nitrogen on the sample surface.

After the first functionalization to yield **CNO-1**, the content of oxygen increases as expected due to the presence of carboxylic moieties on the surface, indicating the functionalization of the CNOs with the benzoic acid units (Figure S3 in the Supporting Information).[42] The successful functionalization of the **CNO-1** was also supported by the analysis of the C1 s core level spectra (Figure 1 A and B). In fact, the fitting of the C1 s core level spectrum of **p-CNO** reveals the presence of the expected sp^2 and sp^3 components (285 and 285.9 eV, respectively) and the large π–π^* satellites at about 291 eV. On the other hand, the functionalization with the 4-amino benzoic acid results in an additional component at about 289 eV (Figure 1 B), which is attributable to the carbon atoms on the carboxylic functionalities.

An increase of the sp^3 component in the spectra of **CNO-1** is also noticed in agreement with the characterization by Raman spectroscopy. XPS investigations performed on the CNO

Table 1. Surface composition of different elements obtained from XPS wide spectra of the CNO samples and their comparison with the precursors.

Sample	C [%][a]	O [%][a]	N [%][a]	Si [%][a]	Ca, Na, S [%][a]
p-CNO	97.7 (1.4)	1.9 (0.1)	0.34	–	–
CNO-1	91.8 (0.8)	6.6 (0.9)	0.9 (0.1)	–	<1
CNO-2a	89 (2.4)	8.5 (1.0)	–	1.8 (0.4)	<1
CNO-5	83 (0.2)	14 (0.6)	1.7 (0.4)	0.35 (0.1)	<1
CNO-4	80 (1.4)	16 (1.4)	2.8 (0.5)	1.2 (0.8)	<1
FA-PEG 4	63.3 (2.2)	23 (0.4)	13.7(0.6)	2.6 (0.9)	<1
FITC-PEG 6	85.6 (3.6)	11.8 (3.4)	0.36 (0.2)	–	1.4 (0.6)

[a] Standard deviation reported in brackets.

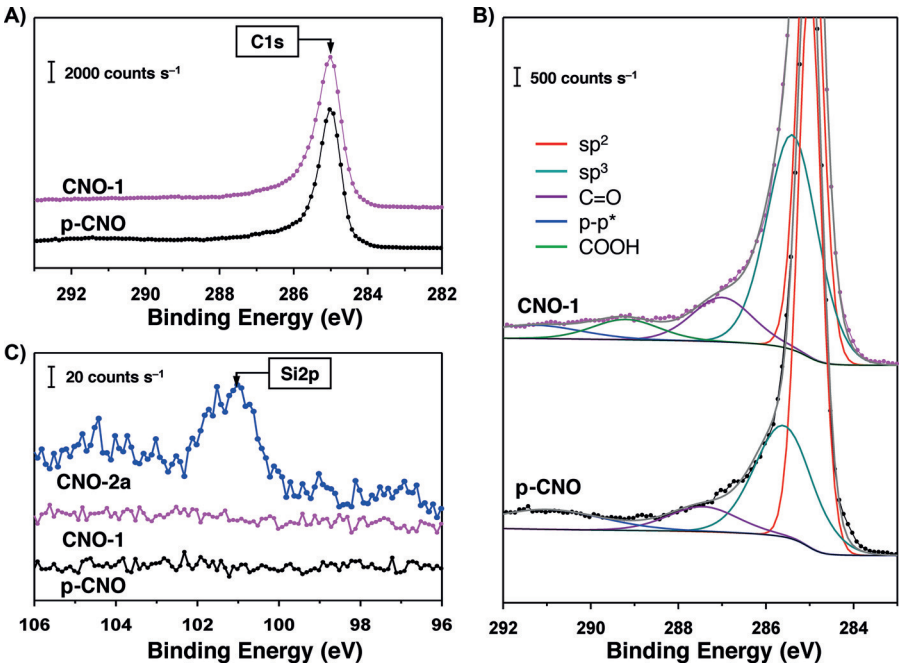

Figure 1. XPS data for the functionalized CNOs. A) XPS C1 s narrow scan of **p-CNO** and **CNO-1**. B) Carbon narrow scan of **p-CNO** and **CNO-1**, including peak-fitting analyses, showing the presence of the peak at about 289 eV corresponding to the carboxylic acid functionalities. C) Si2p narrow scan of **p-CNO**, **CNO-1** and **CNO-2 a**, showing the presence of the silicon peak at 101 eV, indicating the functionalization with the phenylacetylene-TMS of the **CNO-2 a**.

sample after the second reaction (**CNO-2a**) reveal the presence of silicon, indicating the effective functionalization of the surface with the phenylacetylene-TMS group (Figure 1C). An increase of the oxygen signal was also detected; this observation could be explained with the formation of reactive carbon atoms during the diazonium coupling that are keen to adsorb oxygen from the environment. The Raman spectra of **CNO-1** and **CNO-2b** display an enhancement of the D-band (1354 cm^{-1}) normalized with respect to the G-band (1570 cm^{-1}), that indicates the conversion of sp^2 to sp^3 carbons on the surface of CNOs (Figure 2A). The change in the D/G ratio is more evident after the first reaction and an increase from 0.26 for the **p-CNO** to 0.58 for the **CNO-1** was measured. Following the second functionalization, the increase of the D/G ratio is less prominent, a phenomenon that has been previously observed on SWCNTs subjected to multiple diazonium coupling reactions.[43] The chemical modification of **CNO-2b** was also confirmed by FTIR analysis which shows the presence of benzoic acid and phenylacetylene functionalities (Figure 2B). The deprotection of the TMS-alkynyl group upon treatment of **CNO-2a** with TBAF was established from the FTIR spectra of the **CNO-2b** which displays a peak at around 2142 cm^{-1} corresponding to C≡C vibrational modes. Furthermore, the increase of the vibrational bands for C=O (1681 cm^{-1}), and for aromatic C–C bands (1372, 1450, 1538 cm^{-1}) as well as C–H (1020 cm^{-1}) groups indicate the presence of benzoic acid on the surface of **CNO-2b**. Similar features are observed also in the FTIR spectra of **CNO-1**. The FTIR results are in agreement with the XPS data, vouching for the success of the double step functionalization procedure.

The preparation of the CNOs modified with the targeting and imaging agents was realized (Scheme 2 and Supporting Information for detailed synthetic procedures) by two consecutive heterogeneous reactions of **CNO-2b** with the linkers **FA-PEG4** and **FITC-PEG6**. The folic acid derivative **FA-PEG4** was coupled to the benzoic acid groups by using *N*-hydroxysuccinimide (NHS).

The isolated CNOs bearing the folic acid unit (**CNO-3**) were then dispersed in DMF by sonication and treated with the fluorescein derivative **FITC-PEG6** in the presence of $Cu(MeCN)_4PF_6$, 2,6 lutidine and tris(3-hydroxypropyltriazolylmethyl)amine (THPTA) at 50 °C. After reaction, the doubly functionalized **CNO-4** sample was isolated and washed with excess MeOH and H_2O until the fluorescein physically adsorbed on the surface of the modified CNOs was completely removed. Reference CNOs bearing only the fluorescein unit (**CNO-5**) were also prepared following the same synthetic protocol based on the CuAAC reaction starting from **CNO-2b**. The final CNO constructs were characterized by HRTEM, TGA, ToF-SIMS, XPS, FTIR and fluorescence spectroscopies. HRTEM analysis of **CNO-4** shows quasispherical onions with average diameter of 5–7 nm and 6–8 concentric graphitic shells. Further, the structure and the morphology of the particles were retained after surface modification (Figure 3). Comparing the TGA weight loss curves (Figure S1 in the Supporting Information) of **p-CNO** with those after covalent modification with benzoic acid and phenylacetylene moieties, **CNO-2b**, shows a decrease in the decomposition temperature from 721 to 698 °C. The reaction of **CNO-2b** with folic acid derivative to yield **CNO-3** results in a drop of the decomposition temperature to 618 °C, and a further decrease to 588 °C was observed by coupling the fluorescein derivative to obtain **CNO-4**. The weight-loss calculated from the TGA at 500 °C allows the assessment of the degree of functionalization of the CNOs.[44] We estimated about 16 functionalities of folic acid per **CNO-3**, a value that increases to approximately 20 after grafting the fluorescein derivative (Table S1 in the Supporting Information).

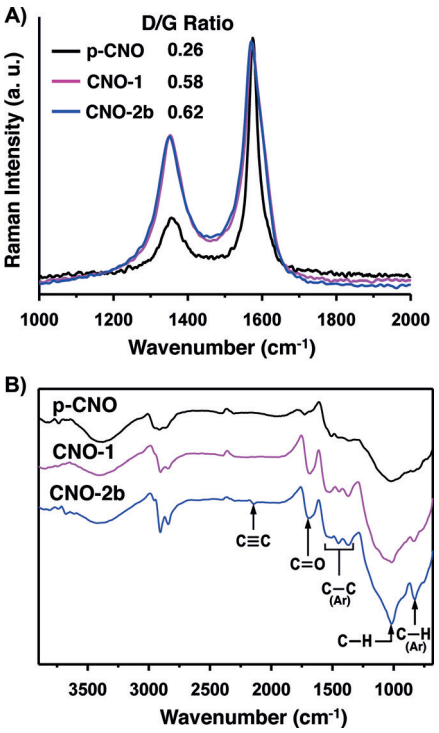

Figure 2. A) Raman analysis, and B) ATR-FTIR spectra of CNOs before, **p-CNO** (black line), and after chemical modification, **CNO-1** (purple line) and **CNO-2b** (blue line). The Raman spectra were focused on the D and G bands at 457 nm excitation wavelength. The ATR-FTIR spectra were accumulated from 64 scans with normal resolution using germanium crystals.

The surface composition of the **CNO-4** was investigated by XPS and ToF-SIMS (Figure 4). Upon reaction of the **FA-PEG4** derivative with **CNO-2b**, an increase of the oxygen is detected from the XPS analysis, as a consequence of the introduction of

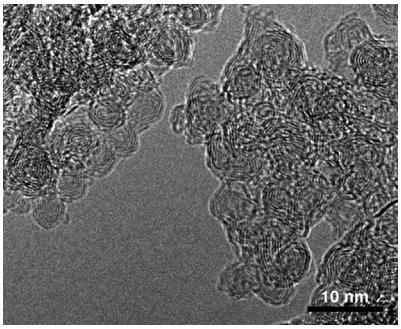

Figure 3. Representative high-resolution TEM image of **CNO-4**.

the PEG chain on the surface (Figure S3 in the Supporting Information). A significant increasing of the nitrogen content was observed after functionalization of the CNOs' surface with **FA-PEG 4** (Figure 4B), even though it was to a lower extent considering the theoretical composition of folic acid. Analysis of the surface chemistry of the **CNO-4** was also performed by ToF-SIMS (Figure 4C–F and Figure S4 in the Supporting Information). For sake of simplicity, only the negative ToF-SIMS spectra are shown although positive spectra were also recorded (Figure S5 in the Supporting Information). The ToF-SIMS analysis was performed with Bi^{3+} source in order to retain the molecular information, as demonstrated in previous studies.[45] The peak at 68 amu (Figure 4C), corresponding to the formula $[C_2N_3H_2]^-$, can be assigned to the triazole that has lost one hydrogen atom.

The presence of this fragment in the TOF-SIMS spectra is the confirmation that the surface attachment of FITC occurred upon click reaction. The peaks detected at 162 amu (Figure 4D) and at 176 amu (Figure 4E) can be ascribed to the pteridine derivatives, respectively, with the formulae $[C_6H_4N_5O]^-$ and $[C_7H_6N_5O]^-$, obtained from the fragmentation of the folic acid. The peak at 211 amu (Figure 4F) could be related to the xantene moiety, $[C_{13}H_7O_3]^-$, of the FITC. The FTIR spectra of **CNO-3** and **CNO-4** were also recorded and the results were compared with the FTIR spectra of the folic acid derivative **FA-PEG 4** and of the fluorescein **FITC-PEG 6** (Figure S6 in the Supporting Information). The successful attachment of the fluorophore was also confirmed by the intense emission ($\lambda_{em} = 540$ nm) observed for a DMF suspension of **CNO-4** upon photoexcitation of the grafted fluorescein units at 495 nm (Figure S7 in the Supporting Information). In comparison with the emission of free fluorescein in solution ($\lambda_{em} = 544$ nm), the fluorescence spectra of **CNO-4** and **CNO-5** are characterized by a shift of the emission maximum, implying a different environment surrounding the fluorophores anchored on the surface of the CNOs.

The cytocompatibility of the functionalized CNOs is a key consideration for use of these nanomaterials as fluorescent probes for cancer cells. The cytotoxicity of the different CNO constructs, including **CNO-1**, **CNO-4** and **CNO-5**, were tested on two different cell lines, the HeLa and KB cells. The cells were treated with a suspension of CNOs at different concentrations (2, 5, 10 and 20 $\mu g\,mL^{-1}$) and the metabolic activity was assessed after different incubation times (Figure 5). The administration of the functionalized CNOs to HeLa cells did not result in significant cytotoxicity as confirmed by the high value of cell viability, which was always more than 85% as compared to the control. The viability of KB cells treated with **CNO-1**, **CNO-4** or **CNO-5** was found to be more than 80% even after 48 h of incubation. However, at the higher concentration of 20 $\mu g\,mL^{-1}$, and longer incubation time, a drop of the viability to 70% was observed for KB cell treated with **CNO-4** and **CNO-5**. In addition to the observed cell viability of the CNO constructs presented in the present study, it should be point out that a low inflammatory response was previously demonstrated both in vitro and in vivo for surface functionalized CNOs.[17] Overall, these results demonstrate a relatively low cytotoxicity of CNOs modified with

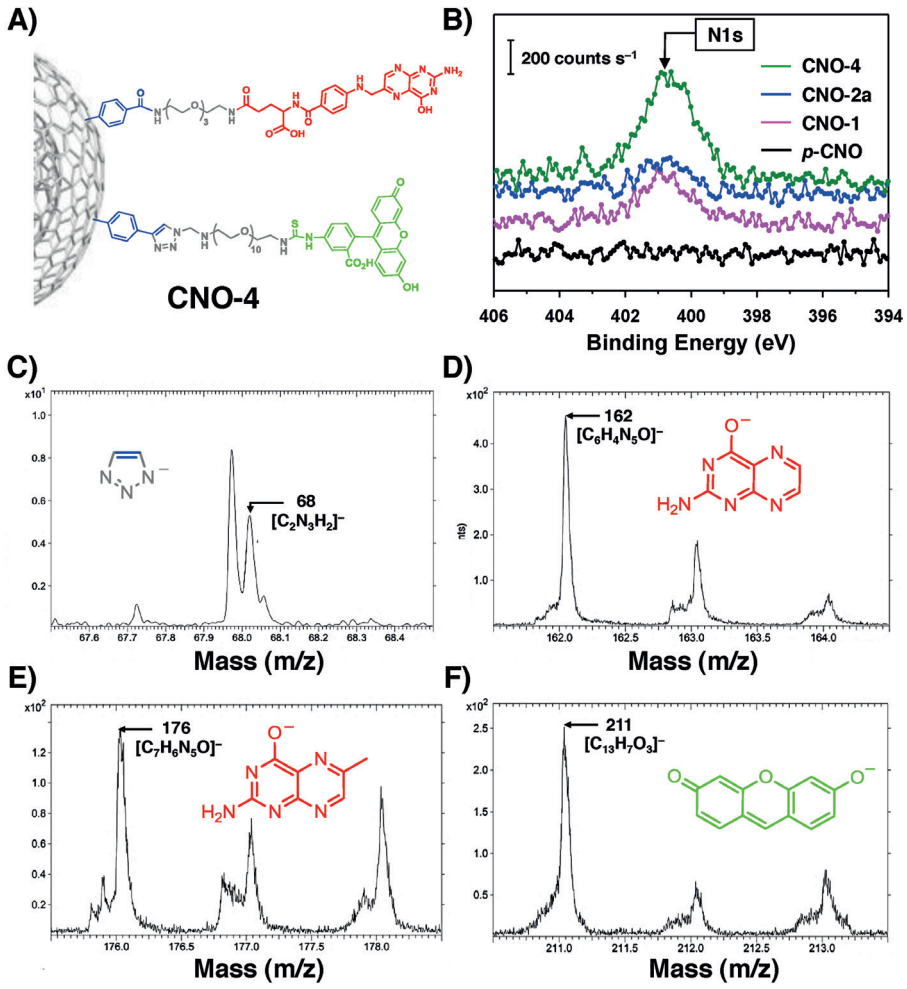

Figure 4. A) Schematic representation of the **CNO-4** with the chemical structures of the modified folic acid unit and fluorescein unit. B) N1s narrow scan of **p-CNO**, **CNO-1**, **CNO-2a** and **CNO-4** showing the presence of the peak at 401 eV corresponding to the N constituent. Negative-ion ToF-SIMS spectra for **CNO-4**, displaying: C) the peak at 68 amu from the triazole ring, D,E) the peak at 162 and 176 amu corresponding to fragmentation of the folic acid unit, and F) the peak at 211 amu corresponding to a fragment of the fluorescein moiety.

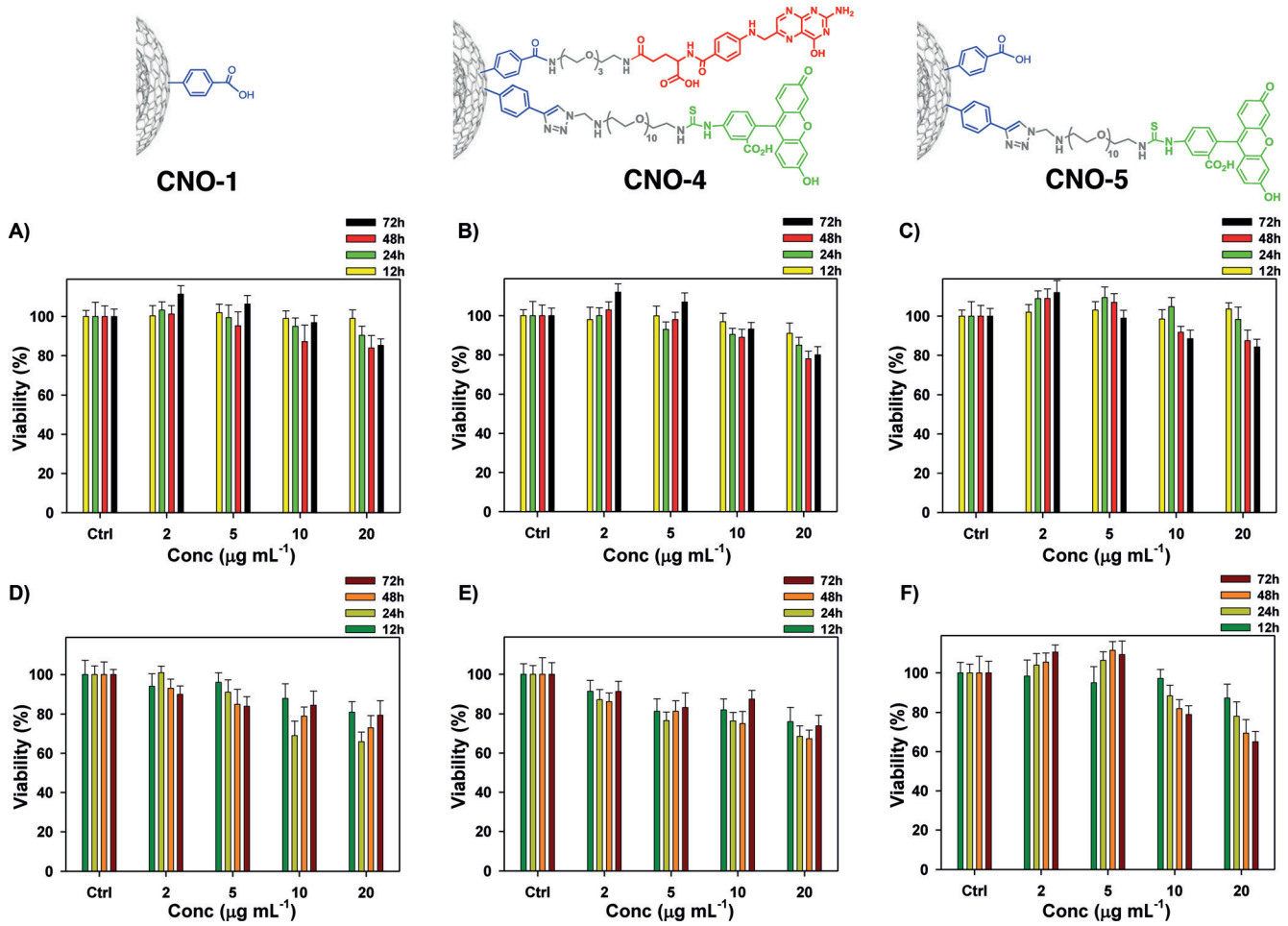

Figure 5. A–C) Cellular viability of HeLa cells, and D–F) KB cells after exposure to 2, 5, 10 and 20 μg mL^{-1} of **CNO-1** (A, D), **CNO-4** (B, E) and **CNO-5** (C, F). The viability of the HeLa and KB cells in the presence of different CNOs was evaluated against a non-treated control. The viability of the cells after exposure to CNO samples was evaluated with a rezoazurin-based assay.

suitable functional groups that encourage the further investigation of these materials as imaging probes for cancer cells.

In order to explore the ability of **CNO-4** and **CNO-5** to enter HeLa and KB cells we performed confocal live cell imaging. After incubating the HeLa cells for 24 h at 37 °C with 10 μg mL^{-1} of **CNO-4**, the imaging probe was clearly internalized by cells (Figure 6 A). Although the green fluorescence signal from **CNO-4** was widely spread inside the cells, a stronger signal could be detected in the cytoplasm and in the perinuclear region, likely due to intravesicle storage of the CNOs. The phase contrast image shows that the HeLa cells remain morphologically healthy after being exposed to **CNO-4** for 24 h. The non-targeted **CNO-5** constructs are also internalized by HeLa cells, as shown from the confocal image in Figure 6 C, although to a lower extend in comparison with the **CNO-4**, as confirmed by the low green fluorescence signal. In order to confirm the localization of the **CNO-4** in the HeLa cells, optical sectioning of the cells by confocal laser scanning microscopy was carried out (Figure S8 in the Supporting Information). The green emission within the cell indicates that the **CNO-4** were internalized by the cells and transported in the perinuclear regions, while no green signal was detected in the nucleus or on the cell membrane.

The localization of the **CNO-4** into lysosomal compartments was assessed by staining the lysosomes with the Lysotracker probe (Figure 7). The intense yellow co-localization signals confirmed that the folic-acid-functionalized **CNO-4** localizes in lysosomal vesicles upon internalization into the cells. With the aim to understand the mechanism for the cellular internalization of CNOs, we performed a correlative imaging analysis (CLEM) for our modified CNOs based on confocal and electron microscopy. With respect to other carbon-based nanomaterials, CNOs are indeed promising markers for electron microscopy experiments in biological samples because the electron-dense multi-shell fullerene core allows their discrimination from carbon-rich cell structures.

The combination of both light and electron microscopy for the imaging of cells treated with **CNO-4** confirmed an endocytosis pathway for the uptake of **CNO-4** (Figure 8 and Figure S9 in the Supporting Information).

TEM analysis of the subcellular regions, where FITC and Lysotracker probes co-localized based on confocal imaging, re-

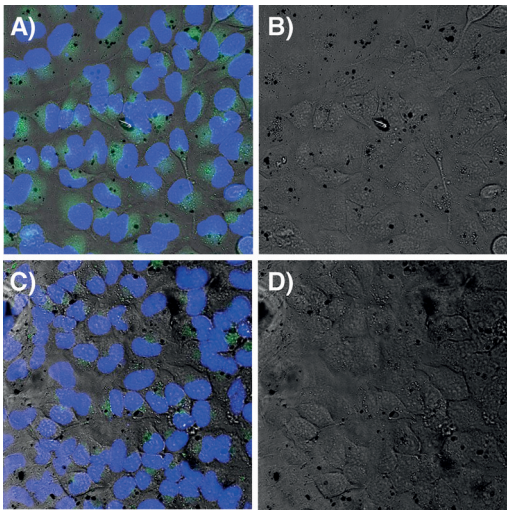

Figure 6. Phase contrast/fluorescence overlay images (A, C) and phase contrast images (B, D) of HeLa cells after incubation for 24 h at 37 °C with 10 μg mL^{-1} of **CNO-4** (A, B) or **CNO-5** (C, D). Cells were stained with Hoechst 33342 (blue).

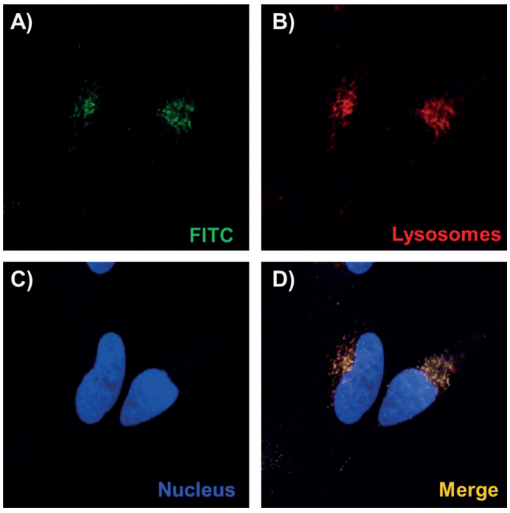

Figure 7. Targeting of HeLa cells with 10 μg mL^{-1} of **CNO-4** incubated for 12 h at 37 °C. A) Green fluorescence from **CNO-4**. B) Lysosomes stained with Lysotracker (red). C) Nucleus stained with Hoechst 33342 (blue). D) Merged image with the co-localization (yellow) of **CNO-4** within the lysosomes.

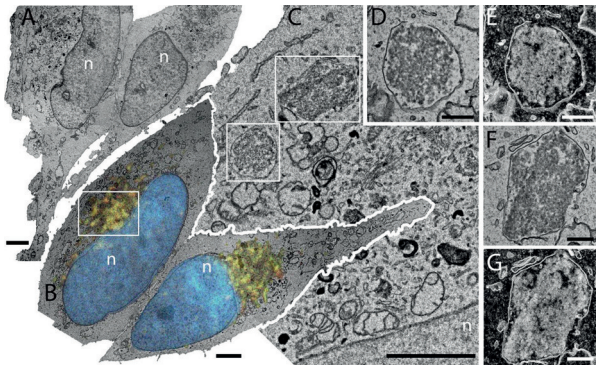

Figure 8. Correlative light electron microscopy analysis of HeLa cells doped with 10 μg mL^{-1} of **CNO-4** for 12 h at 37 °C. A) Low magnification TEM reconstruction of two cells doped with **CNO-4**. B) Superimposed fluorescence and TEM reconstruction of the same cells shown in A (imaged in a different section). The co-localization of **CNO-4** (green fluorescence) within lysosomes stained with Lysotracker (red) results in yellow fluorescence. C) Higher magnification TEM image of the boxed area in B. Note, the two endosomes containing **CNO-4**. D–G) Higher magnification images of the boxed areas from C imaged, respectively, in defocused TEM (D, F) and in high angular annular dark field (HAADF) scanning TEM (E, G). The nuclei are labelled with "n". Scale bars: A, B) 4 μm, C) 2.5 μm, D–G) 0.5 μm.

vealed the presence of large aggregates of CNOs inside late-endosome/lysosome vesicles (Figure 8 and Figure S10 in the Supporting Information). These results also demonstrate that the fluorescein unit remains attached to the CNOs in different subcellular regions with different pH and redox states. Moreover, the suitably functionalized CNO constructs can work as a potential new class of markers for CLEM, a fact that is of significant interest due to the scarcity of suitable markers that are directly visible both with light and with electron microscopy.[46] Particularly, fluorescence-labelled CNOs containing both tags on the same unit, allow a lower background labelling and a better spatially resolved correlation relative to two secondary probes, such as secondary antibody and colloidal gold marker.[47] The small size of CNOs along with their carbon-based composition provides a highly resolved spatial correlation, and can, in principle, minimize some of the artefacts generated by aggregation, such as fluorescence quenching, and lack of targeting of the probes within the cells.[39]

Moreover, the low cytotoxicity of the CNOs and the possibility to anchor targeting and imaging agents on their surface allows the study of cellular processes close to physiological conditions and for long incubation times. For these reasons, functionalized CNOs represent suitable candidates as probes for both confocal and electron microscopy, not only to study their pathways within the cell environment, as we have shown here, but also to investigate the role and function of specific proteins in the cellular processes and regulation. In order to establish the effect of the conjugated folic acid on cell targeting and subsequent internalization of the CNOs, we incubated KB cells, overexpressing folate receptors,[48] with **CNO-4** and **CNO-5** (10 μg mL^{-1}) for a period of 3 h at 37 °C. Confocal images of KB cells exposed to **CNO-4** show well-defined green fluorescence from the fluorescein labelled **CNO-4**, which is mainly collected in the perinuclear region (Figure 9 A). The accumulation of the **CNO-4** in vesicles, as indicated from the strong yellow co-localization signal (Figure 9 A and Figure S11 in the Supporting Information), suggests a folate-mediated endocytosis pathway for the uptake of folate conjugates of CNOs by cancer cells, as observed in previous studies with folic acid functionalized quantum dots[48] or metallic nanoparticles.[49]

Additional evidence for the uptake of **CNO-4** through receptor-mediated endocytosis comes from control experiments where KB cells were incubated in medium with 5 μM free folic acid before the addition of 10 μg mL^{-1} of **CNO-4**. The presence of free folic acid in solution results in minimal internalization of the **CNO-4** as a consequence of the competition for the folate

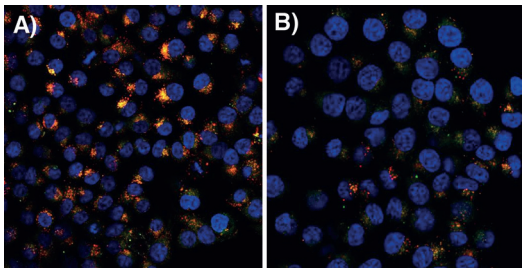

Figure 9. Confocal image of KB cells incubated for 3 h with: A) 10 μg mL^{-1} **CNO-4**, and B) 10 μg mL^{-1} **CNO-5**. Cells were stained with Lysotracker (red) and Hoechst 33342 (blue).

receptors on the cell membranes. Furthermore, when KB cells were incubated with **CNO-5**, the confocal image displayed a lower green signal relative to the fluorescein emission and only a few co-localization regions (Figure 9B). Only after longer incubation times a significant fluorescence from **CNO-5** was detected in the KB cells. It should be noted that a comparable intensity of the fluorescence signal was also observed after a longer incubation time of HeLa cells with 10 μg mL^{-1} of **CNO-5**, an indication that internalization of the non-targeted **CNO-5** occurs by nonspecific adsorption on the cell membrane. Collectively, these results demonstrate that: 1) the internalization of the folic-acid-targeted CNOs occurred through their interaction with the folic acid receptor, and 2) the absence of a specific binding event between the non-targeted fluorescent labelled CNOs and the surface of the cells limit their ability to undergo fast endocytosis.

Conclusions

We have developed a versatile strategy for the surface chemical modification of CNOs with suitable functional groups. The modified CNOs have the capability to target cancer cells and image specific cell compartments. Specifically, we have prepared and characterized doubly functionalized CNOs by introducing benzoic acid and alkyne functionalities, using in situ prepared aryl diazonium salts. These functional groups can be further modified in a site-selective manner through conjugation with fluorescein and folic acid linked to a polyethylene glycol chain.

These multi-functionalized CNOs are internalized by cancer cells without significant cytotoxic effects. In the future and with the aim of testing the efficacy of our CNO constructs as fluorescence as well as electron microscopy markers for correlative analysis, we plan to functionalize them with different fluorophores coupled to specific proteins which follow various sorting pathways once endocytosed, such as for example transferrin (Tf) and epidermal growth factor (EGF).

In summary, we propose multi-functionalized CNOs as promising probes for bioimaging applications: 1) they allow covalent surface functionalization with therapeutics, marker molecules and fluorescent tags, displaying a stable fluorescence response in aqueous solutions; 2) the small size ($\leq$5 nm) and low cytotoxicity do not perturb the cellular process under study; 3) the electron-dense multi-shell fullerene core of the CNOs allows the discrimination of this carbon-nanomaterial from carbon-rich cell structures for electron microscopy studies. The ability to tailor the properties of carbon nano-onions by chemical functionalization with imaging, targeting and therapeutic agents and the possibility to characterize their uptake and pathways within the cell environment will pave the way for future investigations of these multi-functional carbon-based nanomaterials for potential diagnostic applications.

Experimental Section

Materials and methods

All starting materials were purchased from commercial suppliers (Sigma–Aldrich or Fisher) and used without further purification. The synthesis of pristine CNOs (**p-CNO**) was performed as previously described.[50] The procedures for the synthesis of compounds **FA-PEG 4** and **FITC-PEG 6** are provided in the Supporting Information.

Synthesis and characterization

CNO-1: The synthesis was performed according to a reported procedure[26] with some modification. Briefly, 200 mg of **p-CNO** was dispersed in DMF (500 mL) by sonication under N_2 for 1 min at 37 kHz (100%) and for 1 h at 68 kHz (50%). Following the addition of *p*-amino benzoic acid (16.5 g) and isoamyl nitrite (26.8 mL), the reaction mixture was sonicated for an additional 30 min at 68 kHz (50%) and stirred for 16 h at 60 °C under a N_2 atmosphere. The reaction mixture was cooled to room temperature and the supernatant was removed by centrifugation (2100 *g*, 1 h). The sample was dispersed in DMF and the synthetic procedure was repeated twice. The solid was washed with a mixture of DMF/H_2O/HCl (1 M; 9:0.9:0.1), 10% water/DMF, 10% water/methanol and methanol. Finally, the residue was dried under vacuum to yield a black solid.

CNO-2: A dispersion of **CNO-1** (120 mg) was prepared in DMF (250 mL) by sonication under N_2 for 1 min at 37 kHz (100%) and 1 h at 68 kHz (50%). 4-[(Trimethylsilyl)ethynyl]aniline[51] (3.13 g) and isoamyl nitrite (3.21 g) were added and the suspension was further sonicated for 30 min at 68 kHz (50%). The reaction mixture was stirred for 16 h at 60 °C under N_2. After cooling to room temperature, the supernatant was removed by centrifugation (2100 *g*, 1 h). The sample was dispersed in DMF and the synthetic procedure was repeated twice. The solid was washed with a mixture of DMF/H_2O/HCl (1 M; 9:0.9:0.1), 10% water/DMF, 10% water/methanol and methanol. The residue was dispersed in 160 mL of NMP/DMF (1:1) by sonication for 1 min at 37 kHz (100%) and 1 h at 68 kHz (50%). A solution 1 M of tetrabutylammonium fluoride (TBAF, 10 mL) in THF was added and the reaction mixture was stirred at room temperature for 1 h. The supernatant was removed by centrifugation (2100 *g*, 1 h) and the solid was recovered and washed several times with DMF. The residue was dried under vacuum to yield a black solid.

CNO-3: A dispersion of **CNO-2** (70 mg) was prepared in DMF (250 mL) by sonication under N_2 for 1 min at 37 kHz (100%) and 1 h at 68 kHz (50%). 4-Dimethylaminopyridine (DMAP, 250 mg) and *N*-hydroxysuccinimide (NHS, 250 mg) were added to the dispersion and the reaction mixture was further sonicated for 10 min at 68 kHz (50%). 1-Ethyl-3-(3-dimethylaminopropyl) carbodiimide (EDCI, 400 mg) was added to the mixture and, after sonication for 3 h at 68 kHz (50%), **FA-PEG 4** (40 mg) was added, sonicated for

1 h at 68 kHz (50%) and the reaction mixture was stirred at 80 °C for 3 days under N_2. The mixture was cooled to room temperature and the supernatant was removed by centrifugation (2100 *g*, 1 h). The solid was washed with a mixture of DMF, DMF/TEA (9.9:0.1), MeOH/TEA (9.9:0.1), MeOH, MeOH/AcOH (9.9:0.1), MeOH, EtOAc and toluene. The residue was dried under vacuum to yield a black solid.

CNO-4: A dispersion of **CNO-3** (50 mg) was prepared in NMP/DMF (1:1, 160 mL) by sonication under N_2 for 1 min at 37 kHz (100%) and 1 h at 68 kHz (50%). **FITC-PEG 6** (28 mg) was added with $Cu(MeCN)_4PF_6$ (16 mg), 2,6-lutidine (0.4 mL) and THPTA (48 mg). The reaction mixture was heated to 50 °C for 3 days under an N_2 atmosphere. The supernatant was removed by centrifugation (2100 *g*, 1 h) and the residue was washed with DMF, toluene and MeOH and dried by lyophilisation to yield a black solid.

CNO-5: The same general procedure as described for **CNO-4** was used, with 40 mg of **CNO-2**.

The different surface functionalized CNOs were characterized by using high-resolution transmission electron microscopy (HRTEM), thermal gravimetric analysis (TGA), time of-flight secondary ion mass spectrometry (ToF-SIMS), X-ray photoelectron spectroscopy (XPS), attenuated total reflectance Fourier transform infrared (ATRF-TIR) and Raman spectroscopies. The experimental details are reported in the Supporting Information and in previous publications.[45]

Cell culture

The human epidermoid carcinoma cells (KB cells), were cultured in a RPMI medium (folic acid free) supplemented with 1% L-glutamine, 10% heat-inactivated foetal bovine serum (FBS), 100 U mL^{-1} penicillin and 100 mg mL^{-1} streptomycin. Cells were grown in monolayer culture at 37 °C under a 5% CO_2 atmosphere in a humidified environment. HeLa cells were cultured in Dulbecco's modified Eagle's medium (DMEM) supplemented with 1% L-glutamine, 10% heat-inactivated FBS, 100 U mL^{-1} penicillin and 100 mg mL^{-1} streptomycin. Cells were grown in a monolayer culture at 37 °C under 5% CO_2 atmosphere in a humidified environment.

Viability assay

Cells were seeded in 24-well chamber slides at a density of 50000 cells per well and incubated in a 500 μL cell culture medium to obtain a sub-confluent monolayer after 48 h in a humidified atmosphere at 37 °C and 5% CO_2. The cell culture medium was removed and replaced with 500 μL of cell medium with **CNO-1**, **CNO-4** or **CNO-5** at concentrations of 2, 5, 10 and 20 μg mL^{-1}. The CNO samples were prepared by dilution of a concentrated suspension of CNOs that were obtained by suspending 1 mg of sample in 1 mL of sterile phosphate buffered saline (PBS) solution followed by sonication for 20 min at 68 kHz (50%). The metabolic activity for both cell culture lines was measured after 12, 24, 48 and 72 h of exposure to the samples of CNO, utilizing the PrestoBlue cell viability assay (Life Technologies). Assays were performed following a procedure previously described[52] by measuring the absorbance on a microplate reader at a wavelength of 570 nm. Each measurement was normalized with the average signal of untreated wells to determine the percent cell viability expressed as the mean ± SD.

Cellular imaging

Cells were seeded on 25 mm glass-bottom dishes in order to obtain a sub-confluent monolayer (50–60% confluent) after incubation for 48 h in a humidified atmosphere at 37 °C and 5% CO_2. The culture medium was removed and replaced with 10 μg mL^{-1} suspension of **CNO-4** or **CNO-5** for 3, 12 and 24 h. After the incubation period, the medium was removed and the cells were washed with PBS three times. The cells were treated with 100 nM Lysotracker Deep Red (Invitrogen) for 5 min and with nucleus stain Hoechst 33342 for 7 min at 37 °C. The cells were then washed with PBS and fresh medium was added. The samples were transferred to the microscope incubator and the cells were incubated at 37 °C in a humidified atmosphere during the confocal study. Living cell fluorescence imaging was performed with a laser scanning confocal microscope equipped with a resonant scanner (Nikon A1R) using a 20× objective. Excitation of the fluorescein on the CNO samples was performed at 488 nm and the emission was acquired in the spectral window between 500–560 nm. The Lysotracker Deep Red was exited at 577 nm, while the Hoechst 33342 was exited at 405 nm and the images were acquired, respectively, in the emission range of 600–680 nm and 415–480 nm.

CLEM analysis

For confocal and electron microscopy correlative studies, HeLa cells were grown on photoetched glass coverslips (Bellco Glass Inc., USA), incubated for 12 h with 10 μg mL^{-1} of **CNO-4** and stained with Lysotracker Deep Red and Hoechst 33342. After live cell fluorescence imaging, the cells were processed for transmission electron microscopy. Briefly, cells were fixed in situ with 0.1 M cacodylate-buffered 2% glutaraldehyde solution, post-fixed with 1% osmium tetroxide in the same buffer. They were stained, overnight, in the absence of light in a 0.5% aqueous solution of uranyl acetate, dehydrated in a graded ethanol series, and embedded in EPON resin. The embedded cells were released from the etched cover-slip by transferring the sample between liquid nitrogen and hot water. Sections of about 70 nm were cut with a diamond knife (DIATOME) on a Leica EM UC6 ultramicrotome. TEM images were collected with a Jeol Jem 1011 transmission electron microscope, equipped with a W thermionic gun operating at 100 kV of acceleration voltage and recorded with a 2 Mp Gatan Orius SC100 charge-coupled device (CCD) camera.

Acknowledgements

Istituto Italiano di Tecnologia (IIT) and Science Foundation Ireland (SFI) are greatly acknowledged for research funding. We thank Dr. Manuel N. Chaur (University of Texas at El Paso) for CNO synthesis and Tiziano Catelani (IIT) for EM sample preparation and TEM analysis. We also thank the Department of Nanochemistry at IIT for cell culture and electron microscopy facilities and the Nikon Imaging Center at IIT for help with confocal microscopy. S.G. wishes to thank the "L'Oreal UNESCO For Women in Science Fellowship". L.E. wishes to thank the NSF, PREM Program (DNR-1205302 and CHE-1408865), as well as the Robert A. Welch Foundation (Grant AH-0033) for generous support. G.C. and V.S. acknowledge the JRC institutional action "Nanobiosciences".

Keywords: electron microscopy · fluorescence · folate receptor · nanomaterials · surface chemistry

[1] N. Kamaly, A. Xiao, P. M. Valencia, A. F. Radovic-Moreno, O. C. Farokhza, *Chem. Soc. Rev.* **2012**, *41*, 2971.

[2] J. Zhang, P. L. Yang, N. S. Gray, *Nat. Rev. Cancer* **2009**, *9*, 28.

[3] a) S. Gunaseelan, K. Gunaseelan, M. Deshmukh, X. Zhang, P. J. Sinko, *Adv. Drug Delivery Rev.* **2010**, *62*, 518; b) L. N. Ramanaa, A. R. Anand, S. Sethuramana, U. M. Krishnan, *J. Controlled Release* **2014**, *192*, 271.
[4] a) X. Gao, Y. Cui, R. M. Levenson, L. W. K. Chung, S. Nie, *Nat. Biotech.* **2004**, *22*, 969; b) M. E. Davis, Z. Chen, D. M. Shin, *Nat. Rev. Drug Discovery* **2008**, *7*, 771; c) J. M. Montenegro, V. Grazu, A. Sukhanova, S. Agarwal, J. M. de La Fuente, I. Nabiev, A. Greiner, W. J. Parak, *Adv. Drug Delivery Rev.* **2013**, *65*, 677.
[5] J. Hrkach, D. von Hoff, M. Ali, E. Andrianova, J. Auer, T. Campbell, D. de Witt, M. Figa, M. Figueiredo, A. Horhota, S. Low, K. McDonell, E. Peeke, B. Retnarajan, A. Sabnis, E. Schnipper, J. Song, Y. H. Song, J. Summa, D. Tompsett, G. Troiano, T. van Geen, J. Wright, J. P. LoRusso, P. P. Kantoff, N. H. Bander, C. J. Sweeney, O. C. Farokhzad, R. Langer, S. Zale, *Sci. Transl. Med.* **2012**, *4*, 128.
[6] J. L. Delgado, M. A. Herranz, N. Martín, *J. Mater. Chem.* **2008**, *18*, 1417.
[7] a) P. Singh, S. Campidelli, S. Giordani, D. Bonifazi, A. Bianco, M. Prato, *Chem. Soc. Rev.* **2009**, *38*, 2214; b) A. Krueger, in *The Structure and Properties of Carbon Nanotubes* (Ed.: H. Dodziuk), Wiley-VCH, Weinheim, **2009**; c) M. A. Herranz, N. Martín, in *Carbon Nanotubes and Related Structures: Synthesis Characterization, Functionalization, and Applications* (Eds.: D. M. Guldi, N. Martín), Wiley-VCH, Weinheim, **2010**.
[8] a) G. Pastorin, W. Wu, S. Wieckowski, J.-P. Briand, K. Kostarelos, M. Prato, A. Bianco, *Chem. Commun.* **2006**, 1182; b) M. De Nicola, D. Mirabile Gattia, S. Bellucci, G. De Bellis, F. Micciulla, R. Pastore, A. Tiberia, C. Cerella, M. D'Alessio, M. Vittori Antisari, R. Marazzi, E. Traversa, A. Magrini, A. Bergamaschi, L. Ghibelli, *J. Phys. Condens. Matter* **2007**, *19*, 395013; c) F. Lu, L. Gu, M. J. Meziani, X. Wang, P. G. Luo, L. M. Veca, L. Cao, Y.-P. Sun, *Adv. Mater.* **2009**, *21*, 139; d) C. Fabbro, H. Ali-Boucetta, T. Da Ros, K. Kostarelos, A. Bianco, M. Prato, *Chem. Commun.* **2012**, *48*, 3911.
[9] a) R. Marega, F. De Leo, F. Pineux, J. Sgrignani, A. Magistrato, A. D. Naik, Y. Garcia, L. Flamant, C. Michiels, D. Bonifazi, *Adv. Funct. Mater.* **2013**, *23*, 3173; b) S. Wen, Q. Zhao, X. An, J. Zhu, W. Hou, K. Li, Y. Huang, M. Shen, W. Zhu, X. Shi, *Adv. Healthc. Mater.* **2014**, *3*, 1568.
[10] P. W. Barone, S. Baik, D. A. Heller, M. S. Strano, *Nat. Mater.* **2005**, *4*, 86.
[11] D. Movia, A. Prina Mello, D. Bazou, Y. Volkov, S. Giordani, *ACS Nano* **2011**, *5*, 9278.
[12] H. Ali-Boucetta, A. Nunes, R. Sainz, M. A. Herrero, B. Tian, M. Prato, A. Bianco, K. Kostarelos, *Angew. Chem. Int. Ed.* **2013**, *52*, 2130; *Angew. Chem.* **2013**, *125*, 2184.
[13] J. Miyawaki, M. Yudasaka, T. Azami, Y. Kubo, S. Iijima, *ACS Nano* **2008**, *2*, 213.
[14] V. N. Mochalin, O. Shenderova, D. Ho, Y. Gogotsi, *Nat. Nanotechnol.* **2012**, *7*, 11.
[15] a) Y. Liang, M. Ozawa, A. Krueger, *ACS Nano* **2009**, *3*, 2288; b) A. Krueger, D. Lang, *Adv. Funct. Mater.* **2012**, *22*, 890; c) A. Krueger, in *The Chemistry of Nanodiamond* (Ed.: O. A. Williams), RSC, London, **2014**.
[16] a) A. Montellano, T. Da Ros, A. Bianco, M. Prato, *Nanoscale* **2011**, *3*, 4035; b) J. Luczkowiak, A. Munoz, M. Sanchez-Navarro, R. Ribeiro-Viana, A. Ginieis, B. M. Illescas, N. Martín, R. Delgado, J. Rojo, *Biomacromolecules* **2013**, *14*, 431.
[17] M. Yang, K. Flavin, G. Radics, C. H. A. Hearnden, G. J. McManus, B. Moran, A. Villalta-Cerdas, L. A. Echegoyen, S. Giordani, E. C. Lavelle, *Small* **2013**, *9*, 4194.
[18] B. Mu, J. Zhang, T. P. McNicholas, N. F. Reuel, S. Kruss, M. S. Strano, *Acc. Chem. Res.* **2014**, *47*, 979.
[19] J. Bartelmess, S. J. Quinn, S. Giordani, *Chem. Soc. Rev.* **2015**, *44*, 4672.
[20] G. Hong, S. Diao, A. L. Antaris, H. Dai, *Chem. Rev.* **2015**, *115*, 10816.
[21] J. L. Bahr, J. Yang, D. V. Kosynkin, M. J. Bronikowski, R. E. Smalley, J. M. Tour, *J. Am. Chem. Soc.* **2001**, *123*, 6536.
[22] A. Battigelli, C. Ménard-Moyon, T. Da Ros, M. Prato, A. Bianco, *Adv. Drug Delivery Rev.* **2013**, *65*, 1899.
[23] *Supramolecular Chemistry of Fullerenes and Carbon Nanotubes* (Eds.: N. Martín, J.-F. Nierengarten), Wiley-VCH, Weinheim, **2012**.
[24] a) C. Ménard-Moyon, C. Fabbro, M. Prato, A. Bianco, *Chem. Eur. J.* **2011**, *17*, 3222; b) G. Tuci, L. Luconi, A. Rossin, F. Baldini, S. Cicchi, S. Tombelli, C. Trono, A. Giannetti, I. Manet, S. Fedeli, A. Brandi, G. Giambastiani, *ChemPlusChem* **2015**, *80*, 704; c) C. Ménard-Moyon, H. Ali-Boucetta, C. Fabbro, O. Chaloin, K. Kostarelos, A. Bianco, *Chem. Eur. J.* **2015**, *21*, 14886.
[25] T. Meinhardt, D. Lang, H. Dill, A. Krueger, *Adv. Funct. Mater.* **2011**, *21*, 494.
[26] L. Echegoyen, A. Ortiz, M. N. Chaur, A. J. Palkar, in *Chemistry of Nanocarbons* (Eds.: T. Akasaka, F. Wudl, S. Nagase), Wiley, Hoboken, **2010**.
[27] a) L. Zhou, C. Gao, D. Zhu, W. Xu, F. F. Chen, A. Palkar, L. Echegoyen, E. S. Kong, *Chem. Eur. J.* **2009**, *15*, 1389; b) K. Flavin, M. N. Chaur, L. Echegoyen, S. Giordani, *Org. Lett.* **2010**, *12*, 840; c) M. E. Plonska-Brzezinska, J. Mazurczyk, B. Palys, J. Breczko, A. Lapinski, A. T. Dubis, L. Echegoyen, *Chem. Eur. J.* **2012**, *18*, 2600; d) A. Molina-Ontoria, M. N. Chaur, M. E. Plonska-Brzezinska, L. Echegoyen, *Chem. Commun.* **2013**, *49*, 2406; e) J. Bartelmess, S. Giordani, *Beilstein J. Nanotechnol.* **2014**, *5*, 1980; f) J. Bartelmess, M. Baldrighi, V. Nardone, E. Parisini, D. Buck, L. Echegoyen, S. Giordani, *Chem. Eur. J.* **2015**, *21*, 9727.
[28] J. Bartelmess, E. De Luca, A. Signorelli, M. Baldrighi, M. Becce, R. Brescia, V. Nardone, E. Parisini, P. P. Pompa, L. Echegoyen, S. Giordani, *Nanoscale* **2014**, *6*, 13761.
[29] S. Giordani, J. Bartelmess, M. Frasconi, I. Biondi, S. Cheung, M. Grossi, D. Wu, L. Echegoyen, D. O'Shea, *J. Mater. Chem. B* **2014**, *2*, 7459.
[30] Y. Lu, P. S. Low, *Adv. Drug Delivery Rev.* **2002**, *54*, 675.
[31] H. Elnakat, M. Ratnam, *Adv. Drug Delivery Rev.* **2004**, *56*, 1067.
[32] P. S. Low, W. A. Henne, D. D. Doorneweerd, *Acc. Chem. Res.* **2008**, *41*, 120.
[33] a) M. E. Werner, J. A. Copp, S. Karve, N. D. Cummings, R. Sukumar, C. Li, M. E. Napier, R. C. Chen, A. D. Cox, A. Z. Wang, *ACS Nano* **2011**, *5*, 8990; b) N.-C. Fan, F.-Y. Cheng, J.-A. Ho, C.-S. Yeh, *Angew. Chem. Int. Ed.* **2012**, *51*, 8806; *Angew. Chem.* **2012**, *124*, 8936; c) X. Ma, Y. Zhao, K. Woei Ng, Y. Zhao, *Chem. Eur. J.* **2013**, *19*, 15593.
[34] S. A. Kularatne, V. Deshmukh, M. Gymnopoulos, S. L. Biroc, J. Xia, S. Srinagesh, Y. Sun, N. Zou, M. Shimazu, J. Pinkstaff, S. Ensari, N. Knudsen, A. Manibusan, J. Y. Axup, C. H. Kim, V. V. Smider, T. Javahishvili, P. G. Schultz, *Angew. Chem. Int. Ed.* **2013**, *52*, 12101; *Angew. Chem.* **2013**, *125*, 12323.
[35] a) J. Geng, K. Li, K.-Y. Pu, D. Ding, B. Liu, *Small* **2012**, *8*, 2421; b) L. Sun, Z. Wei, H. Chen, J. Liu, J. Guo, M. Cao, T. Wen, L. Shi, *Nanoscale* **2014**, *6*, 8878; c) A. Topete, M. Alatorre-Meda, E. M. Villar-Alvarez, S. Carregal-Romero, S. Barbosa, W. J. Parak, P. Taboada, V. Mosquera, *Adv. Healthcare Mater.* **2014**, *3*, 1309.
[36] M. E. Wagner, T. A. Horbett, D. G. Castner, *Langmuir* **2003**, *19*, 1708.
[37] F. Brétagnol, A. Valsesia, G. Ceccone, P. Colpo, D. Gilliland, L. Ceriotti, M. Hasiwa, F. Rossi, *Plasma Processes Polym.* **2006**, *3*, 443.
[38] J. C. Vickerman, I. S. Gilmore, *Surface Analysis: The Principal Techniques*, 2nd ed., Wiley, Hoboken, **2009**.
[39] E. Sacher, *Langmuir* **2010**, *26*, 3807.
[40] D. R. Baer, D. J. Gaspar, P. Nachimuthu, S. D. Techane, D. G. Castner, *Ann. Bioanal. Chem* **2010**, *396*, 983.
[41] J. Caplan, M. Niethammer, R. M. Taylor II, K. J. Czymmek, *Curr. Opin. Struct. Biol.* **2011**, *21*, 686.
[42] The content of oxygen observed from the XPS analysis exceeds the expected value. This result could be ascribed to possible contamination during the sample preparation and drying.
[43] D. Tasis, N. Tagmatarchis, A. Bianco, M. Prato, *Chem. Rev.* **2006**, *106*, 1105.
[44] The organic functionalities on the surface of the modified CNOs are considered to be completely decomposed at temperature of 500 °C; the amount of organic materials on the CNOs can be calculated from the weight loss at this temperature.
[45] V. Spampinato, S. Giordani, G. Ceccone, *Biointerphases* **2015**, *10*, 019006.
[46] E. Brown, P. Verkade, *Protoplasma* **2010**, *244*, 91.
[47] L. Hodgson, J. Tavaré, P. Verkade, *Protoplasma* **2014**, *251*, 403.
[48] R. Di Corato, N. C. Bigall, A. Ragusa, D. Dorfs, A. Genovese, R. Marotta, L. Manna, T. Pellegrino, *ACS Nano* **2011**, *5*, 1109.
[49] X. Li, H. Zhou, L. Yang, G. Du, A. S. Pai-Panandiker, X. Huang, B. Yan, *Biomaterials* **2011**, *32*, 2540.
[50] V. L. Kuznetsov, M. N. Aleksandrov, I. V. Zagoruiko, A. L. Chuvilin, E. M. Moroz, V. N. Kolomiichuk, *Carbon* **1991**, *29*, 665.
[51] P. R. Serwinski, P. M. Lahti, *Org. Lett.* **2003**, *5*, 2099.
[52] J. V. Jokerst, A. J. Cole, D. van de Sompel, S. S. Gambhir, *ACS Nano* **2012**, *6*, 10366.

Received: August 11, 2015
Published online on November 18, 2015